IJMMM International Journal of Minerals, Metallurgy and Materials 矿物冶金与材料学报（英文版）

Microwave fluidization magnetization roasting of limonite ores: Phase transformation, microstructure and kinetics

Xinran Zhu, Yuangan Chen, Xu Liu, Yongsheng Sun, and Yuexin Han

Cite this article as:
Xinran Zhu, Yuangan Chen, Xu Liu, Yongsheng Sun, and Yuexin Han, Microwave fluidization magnetization roasting of limonite ores: Phase transformation, microstructure and kinetics, *Int. J. Miner. Metall. Mater.*, 32(2025), No. 7, pp. 1519-1528. https://doi.org/10.1007/s12613-024-3018-1

INTERNATIONAL JOURNAL OF
Minerals, Metallurgy and Materials

Volume 32, Number 7, July 2025
Page 1519

Research Article https://doi.org/10.1007/s12613-024-3018-1

Microwave fluidization magnetization roasting of limonite ores: Phase transformation, microstructure and kinetics

Xinran Zhu[1,2], *Yuangan Chen*[1,2,✉], *Xu Liu*[1,2], *Yongsheng Sun*[1,2], *and Yuexin Han*[1,2]

1) School of Resources and Civil Engineering, Northeastern University, Shenyang 110819, China
2) National-Local Joint Engineering Research Center of High-Efficient Exploitation Technology for Refractory Iron Ore Resources, Shenyang 110819, China
(Received: 1 August 2024; revised: 29 September 2024; accepted: 8 October 2024)

Abstract: As a refractory iron ore, the clean and efficient beneficiation of limonite is crucial for ensuring a sustainable long-term supply of iron metal. In this study, the microwave fluidization magnetization roasting of limonite was explored. The micromorphology, microstructure, and mineral phase transformation of the roasted products were analyzed using a scanning electron microscope, an automatic surface area and porosity analyzer, an X-ray diffractometer, and a vibrating sample magnetometer. Kinetic analysis was also conducted to identify the factors limiting the roasting reaction rate. Microwave fluidization roasting significantly increased the specific surface area of limonite, increased the opportunity of contact between CO and limonite, and accelerated the transformation from FeO(OH) to α-Fe_2O_3 and then to Fe_3O_4. In addition, the water in the limonite ore and the newly formed magnetite exhibited a strong microwave absorption capacity, which has a certain activation effect on the reduction roasting of limonite. The saturation magnetization and maximum specific magnetization coefficient increased to 23.08 $A{\cdot}m^2{\cdot}kg^{-1}$ and 2.50 × 10^{-4} $m^3{\cdot}kg^{-1}$, respectively. The subsequent magnetic separation of the reconstructed limonite yielded an iron concentrate with an Fe grade of 59.26wt% and a recovery of 90.07wt%. Kinetic analysis revealed that the reaction mechanism function model was consistent with the diffusion model ($G(\alpha) = \alpha^2$), with the mechanism function described as $k = 0.08208\exp[-20.3441/(R_gT)]$. Therefore, microwave fluidization roasting shows significant potential in the beneficiation of limonite, offering a promising approach for the exploitation of refractory iron ores.

Keywords: iron ore; separation; reduction roasting; microwave heating; kinetics

1. Introduction

Steel is the backbone of construction, bridges, and transportation infrastructure, playing a crucial role in driving economic and industrial activities [1–3]. Iron metal, the primary raw material for steelmaking, has long held the top position in global metal production and consumption. According to the World Steel Association, world iron and steel production in 2023 reached as high as 1309 million and 1892 million tons, respectively. Iron ore is the primary source of metallic iron; with the increasing depletion of high-quality iron ore resources, the mining of refractory iron ores has become increasingly important in maintaining a regular supply of iron ore [4–5]. High-quality iron ore can be processed into qualified iron concentrate through methods such as gravity separation, magnetic separation, flotation, or even just crushing and screening. For refractory iron ores, additional processing is necessary to effectively enrich the iron content [6–8].

Limonite is a mineral aggregate formed by the weathering of iron sulfide minerals, iron carbonate minerals, and iron-rich silicate minerals [9]. It primarily consists of iron oxides (hematite and goethite) and is a refractory iron ore widely distributed in supergene environments [10]. Its high crystalline water content, loose structure, and susceptibility to slimming make it difficult to process goethite using conventional beneficiation methods [11]. Furthermore, the high content of impurities, such as phosphorus, aluminum, and silicon dioxide, contributes to the difficulty in obtaining qualified iron concentrate [12]. Magnetic separation is the most conventional method for the preenrichment of iron ores; however, limonite is a weak magnetic mineral, and direct magnetic separation is not an optimal approach for this iron ore. Transforming limonite into a strong magnetic mineral through heat treatment to enhance the magnetic separation effect is an effective method for the production of qualified iron concentrate. Fluidization roasting, also known as suspension roasting [13], fluidized bed roasting [14], and flash roasting [15], is currently the main research direction to improve the heat and mass transfer efficiency of the roasting process and has been successfully applied in industrial production [16–17]. In this process, the material is in a fluidized state in the roaster. Liu *et al.* [11] conducted fluidization roasting and magnetic separation on limonite by utilizing H_2 as the reducing gas. Roasting at 798 K and H_2 concentration of 20vol% for 10 min and subsequent weak magnetic separation produced an iron concentrate with an Fe grade of 59.92wt% and a re-

✉ Corresponding author: Yuangan Chen E-mail: yuanganchen@126.com

covery of 87.26wt%. Tang *et al.* [18] and Sun *et al.* [19] employed suspension magnetization roasting, regrinding, and magnetic separation to treat limonite using H_2 and CO as reducing gases. The magnetic separation of the roasting products yielded iron concentrates with Fe recoveries exceeding 94wt%. For the high content of harmful elements such as phosphorus and sulfur in the concentrate from magnetic separation, flotation is a viable technique for their removal.

To date, the enhancement of ore magnetism in an efficient and environmentally sustainable way remains the primary challenge in limonite processing [20–22]. The fluidization roasting of iron ores using H_2 as the reducing gas has improved the roasting efficiency to a certain level and reduced carbon emissions [23–24]. However, the thermal energy utilization rate is still low. Microwave heating is an effective way to address the low thermal energy utilization rate in roasting [25]. Microwave heating uses electromagnetic waves with a frequency of 300 GHz to 300 MHz to interact directly with substances at the molecular level, thereby causing changes in the electric and magnetic fields of the substances and generating heat [26]. Compared with traditional fuel heating, microwave heating offers several advantages, including rapid heating rate, selectivity, and environmental friendliness [27–28]. To reduce carbon emissions, the pyrometallurgical industry urgently requires a low-energy-consumption heating method to help achieve carbon peak and carbon neutrality [29–30]. Roy *et al.* [31] studied the microwave-assisted reduction roasting of titano-magnetite ore and goethitic ore; the titano-magnetite ore was roasted under a power of 5 kW and a coal-to-ore mass ratio of 0.2 for 15 min and then subjected to magnetic separation to obtain an iron concentrate with an iron grade of 62.57wt% and a recovery of 60.01wt%. Meanwhile, the recovery of goethitic ore was 16.80wt% under the same conditions. Mixing magnetite in goethitic ore can improve the effect of wave absorption and thus strengthen the reduction roasting [31]. Zhou *et al.* [32] used microwave heating to roast oolitic hematite and found that microwave treatment promoted the formation of microcracks between ore phases, which was beneficial to roasting and magnetic separation. Wu *et al.* [33] microwave-roasted limonite at 473 K and 600 W with 5% alkali lignin for 30 min and obtained an iron concentrate with 88.72wt% magnetic iron and 82.92wt% iron recovery, showing that microwave-assisted heating effectively reduced the energy consumption of roasting.

Water has an activation effect during microwave roasting [34–35]. Limonite is an iron ore with high water content and thus can be subjected to fluidization roasting through microwave heating. This study proposed to treat limonite with microwave fluidization magnetization roasting. The principal reactions and limiting factors in limonite roasting were analyzed by thermodynamic calculations. The mineral phase reconstruction products, surface microstructure, and magnetic properties of the roasted products of limonite were analyzed by an X-ray diffractometer (XRD), a scanning electron microscope combined with an energy-dispersive spectroscope (SEM–EDS), an automatic dynamic N_2 adsorption specific surface area analyzer, and a vibrating sample magnetometer (VSM). A weak magnetic separation experiment was performed to assess the effectiveness of magnetization roasting.

2. Experimental

2.1. Materials

The limonite ore used in this experiment was obtained from Yunnan province, China. The raw ore was crushed and ground to pass a 1 mm standard Taylor screen and then used for roasting and characterization. XRD was conducted on the sample to determine its principal components, and the results are shown in Fig. 1(a). XRD analysis indicates that the principal iron-bearing minerals are hematite (α-Fe_2O_3) and goethite [FeO(OH)], and the principal gangue mineral is quartz (SiO_2). A chemical multielement analysis was conducted to further determine the chemical composition of the ore sample, and the results are shown in Table 1. The Fe grade is only 32.89wt%, and the contents of harmful elements CaO,

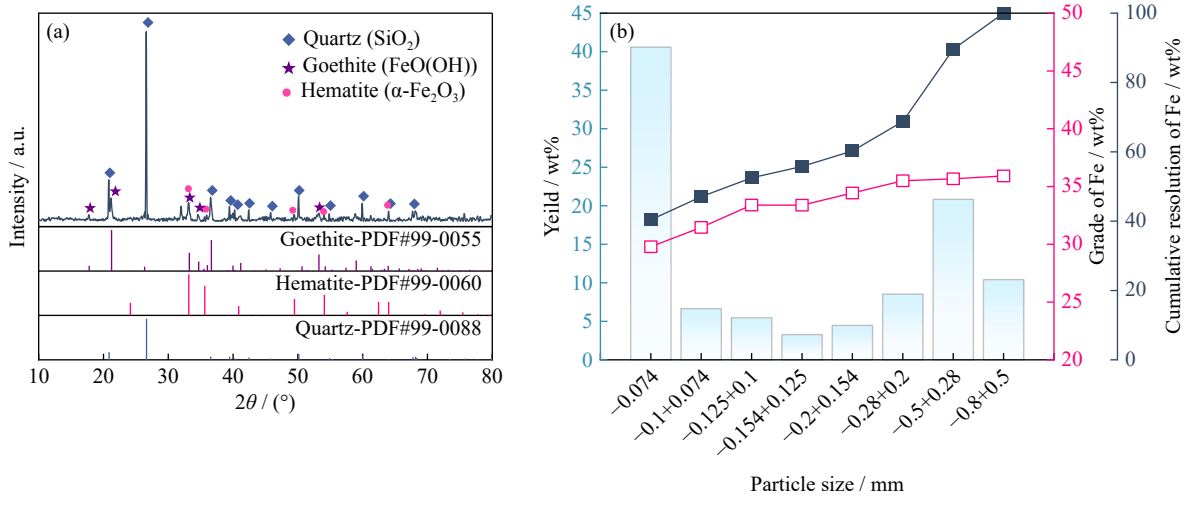

Fig. 1. Results of XRD (a) and particle size composition analysis (b) of the raw ore.

Table 1. Chemical composition of the raw ore wt%

TFe	FeO	SiO_2	MgO	CaO	Al_2O_3	Na	K	P	S	LOI
32.89	0.10	33.88	0.35	1.83	1.46	0.08	0.31	1.22	0.22	8.83

P, and S are 1.83wt%, 1.22wt%, and 0.22wt%, respectively. The loss on ignition (LOI) of the ore sample is 8.83wt%. The ore sample was analyzed for iron chemical phases to clarify the iron distribution, and the results show that the percentages of iron in hematite/limonite, magnetic iron, iron sulfide, iron carbonate, and iron silicate are 98.45wt%, 0, 0.18wt%, 0.52wt%, and 0.85wt%, respectively.

Fluidization magnetization roasting is a process in which ore particles are fluidized by a gas flow, ensuring full contact with the reducing gas. The particle size of the ore has a significant impact on the fluidization effect. The particle size distribution of the ore samples is shown in Fig. 1(b). The ore samples with particle sizes of −0.074 and −0.5+0.28 mm have the highest yield, accounting for 40.58wt% and 20.82wt%, respectively. The −0.8+0.5 and −0.5+0.28 mm particle size fractions have high Fe grades at above 35wt% for both, and their distributions are 11.32wt% and 23.12wt%, respectively. A large portion of the iron is present in the coarse particles. Iron-bearing minerals are encapsulated in gangue minerals, which may require grinding operations in subsequent experiment operations. In addition, the occurrence state of iron in the minerals has a significant impact on the subsequent magnetic separation. A composition analysis of iron was conducted to determine its occurrence state in the raw ore. The results show that the Fe in hematite and goethite accounts for 98.45wt%, with a small portion occurring in siderite and iron silicate.

2.2. Experimental procedure and equipment

Magnetization roasting experiments were conducted using a self-designed microwave fluidization roasting system with an automatic gas mixture supply and temperature control device. For each experiment, 15.00 g of sample was weighed and placed into a quartz tube, where N_2 was introduced to remove air. N_2–CO (20vol% CO, 600 mL·min^{-1}) mixed gas was then introduced, and the microwave power was adjusted to initiate the heating treatment. After the preset temperature was reached, the system automatically reduced the microwave power to maintain a constant temperature for microwave fluidization magnetization roasting. Upon completion of the sample roasting, heating and CO gas supply were ceased, but N_2 introduction was continued. The quartz tube containing the roasted product was then removed from the roaster and allowed to cool in an N_2 atmosphere until room temperature was reached. Subsequent grinding–magnetic separation experiments were conducted to separate iron-bearing minerals from gangue minerals and obtain the final magnetic concentrate. The experimental equipment is shown in Fig. 2. A rod mill (XMB70, Wuhan Exploration Machinery Co., Ltd., China) and a Davis magnetic tube (XCGS type, Wuhan Exploration Machinery Co., Ltd., China) were used for the grinding and magnetic separation experiments, respectively.

2.3. Material characterization methods

The mineral phases of the samples were characterized using an X'Pert pro-MPD system XRD (D8 Advance, Bruker, Germany) at a scanning speed of 10°/min. Their magnetic parameters were examined using a VSM (JDAW-2000D, Yingpu Magnetoelectric, China), and their microscopic morphologies were visualized using SEM–EDS (Ultra Plus, Zeiss, Germany). Their pore parameters in a N_2 atmosphere were studied using an automatic surface area and porosity analyzer (ASAP 2460, Micromeritics, American). The methods used to quantify the chemical composition of the ores are shown in Table S1.

2.4. Thermodynamic and kinetic analysis methods

The composition of limonite ore is complex, and the application of thermodynamic analysis in a nonstandard state

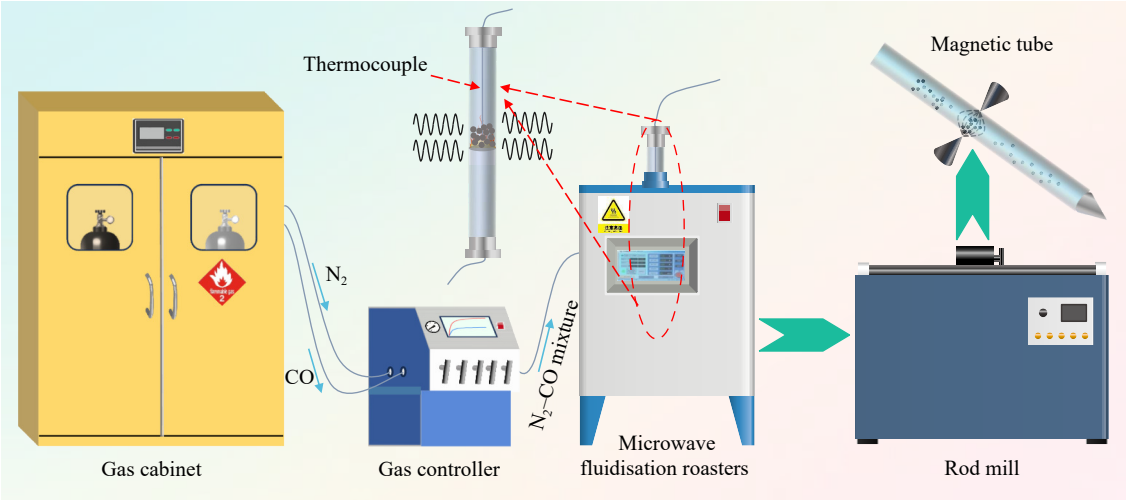

Fig. 2. Schematic of experimental equipment.

would present significant challenges. This study assumes that limonite ore occurs in the standard state so that a thermodynamic study can be performed to provide guidance for practical applications. The software used included FactSage 8.1 and HSC Chemistry 6.0 for calculating the standard Gibbs free energy change ($\Delta_r G_m^{\ominus}$) and reaction enthalpies ($\Delta H^{\ominus}$) of each reaction of limonite in CO and N_2 environments and the equilibrium composition of each component during the reaction.

In this study, the conversion degree (α) of the reaction was determined by assaying the FeO grade of the products with different roasting times, and the reaction rate (v) was obtained by differentiating α with respect to time as shown in Eqs. (1) and (2) [36]. The exact procedure for calculating α was described in the supplementary text. The Arrhenius formula is an empirical formula used to describe the relationship between the rate constant of a chemical reaction and temperature. It was employed in this experiment to describe the kinetic process and determine the kinetic parameters as shown in Eqs. (3) and (4) [37]. The mechanism function of the reaction can be obtained using the integral method in Eq. (5), which gives a linear relationship between $G(\alpha)$ and time (t) for certain roasting temperature conditions [11,38].

$$\alpha = \frac{m_0 - m_t}{m_0 - m_e} \tag{1}$$

$$v = \frac{d\alpha}{dt} \tag{2}$$

$$\frac{d\alpha}{dt} = k(T) f(\alpha) \tag{3}$$

$$k(T) = A \exp\left(-\frac{E_a}{R_g T}\right) \tag{4}$$

$$G(\alpha) = \int_0^{\alpha} \frac{d\alpha}{f(\alpha)} = \int_0^t k(T) dt = k(T) t \tag{5}$$

where m_0, m_t, and m_e are the initial mass of the sample, the mass during the reaction, and the mass after the reaction, respectively, g; $k(T)$ is the kinetic rate constant, s^{-1}; $f(\alpha)$ is the differential form of the kinetic mechanism function in Table S2; T is the roasting temperature, K; A is the preexponential factor, s^{-1}; E_a is the apparent activation energy, $kJ \cdot mol^{-1}$; R_g is the molar gas constant, 8.341 $J \cdot mol^{-1} \cdot K^{-1}$; $G(\alpha)$ is the integral form of the kinetic mechanism function in Table S2.

3. Results and discussion

3.1. Thermodynamic analysis

Roasting thermodynamics is primarily based on the first and second laws of thermodynamics, which are used to determine the feasibility, direction, and limitations of the reaction to achieve control or create conditions that will steer the reaction in the expected direction. Thermodynamic analysis is a method that affects external conditions such as temperature, reactor concentration, and pressure in the reaction system. The reducing gas used in this experiment is CO, and the reactions represented by Eqs. (6)–(11) mainly occur during the magnetization roasting of limonite [18,39–40]:

$$2FeO(OH) = \alpha\text{-}Fe_2O_3 + H_2O(g) \tag{6}$$

$$\alpha\text{-}Fe_2O_3 \cdot H_2O = \alpha\text{-}Fe_2O_3 + H_2O(g) \tag{7}$$

$$3\alpha\text{-}Fe_2O_3 + CO(g) = 2Fe_3O_4 + CO_2(g) \tag{8}$$

$$Fe_3O_4 + CO(g) = 3FeO + CO_2(g) \tag{9}$$

$$Fe_3O_4 + 4CO(g) = 3Fe + 4CO_2(g) \tag{10}$$

$$FeO + CO(g) = Fe + CO_2(g) \tag{11}$$

Fig. 3 shows that when the temperature exceeds 373 K, the dehydration reactions of goethite and hematite exhibit $\Delta_r G_m^{\ominus} < 0$, indicating that these reactions can proceed spontaneously and are endothermic. The dehydration of goethite and hematite provides homogeneous material α-Fe_2O_3 for subsequent magnetic roasting. α-Fe_2O_3 is reduced by CO to form Fe_3O_4, with $\Delta_r G_m^{\ominus} < 0$, indicating that this reaction is also spontaneous and exothermic. As the temperature increases, $\Delta_r G_m^{\ominus}$ continues to decrease, indicating the increasing tendency of α-Fe_2O_3 to be reduced by CO to magnetic mineral Fe_3O_4. Under certain conditions, Fe_3O_4 may undergo the reactions represented by Eqs. (9)–(11) and be further reduced by CO to produce FeO and Fe. When the temperature gradually increases, the $\Delta_r G_m^{\ominus}$ for Eqs. (10) and (11) begins to increase above 0, indicating that these reactions are likely to proceed in the reverse direction with the increasing temperature.

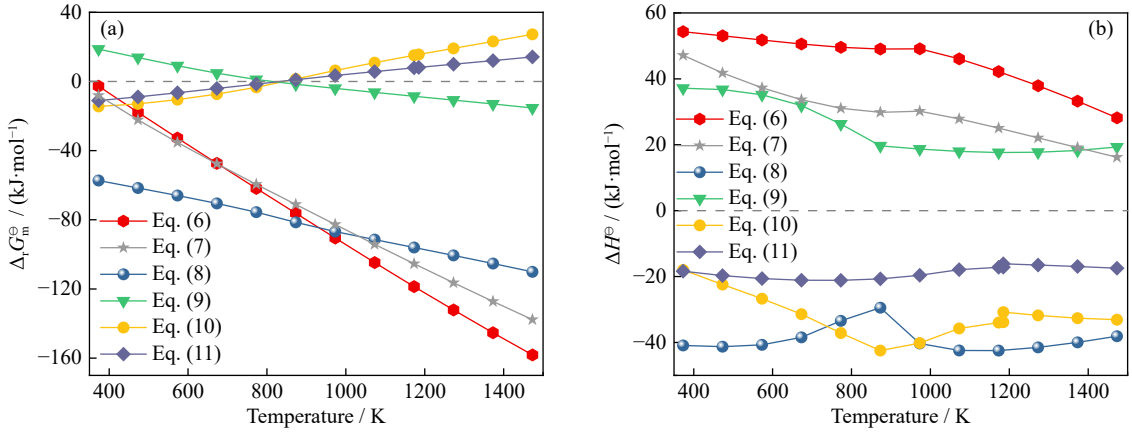

Fig. 3. $\Delta_r G_m^{\ominus}$ (a) and $\Delta H^{\ominus}$ (b) of limonite roasting reactions.

3.2. Microscopic morphology and microstructure evaluation

SEM tests were conducted on the samples before and after roasting to reveal the microscopic morphology of limonite, and the results are shown in Fig. 4. The embedding relationship of the raw ore is relatively complicated, with limonite mainly encapsulated within quartz and apatite particles. Further improving the liberation degree of minerals through grinding is necessary to achieve an effective separation of iron ore and chalcopyrite minerals. Fig. 4(b) indicates that after roasting for 5 min at a temperature of 773 K, the limonite particles exhibit a large number of cracks and pores and a loose porous structure. The two main reasons for the generation of cracks and pores are as follows: the rapid absorption of microwaves by the water in the ore and the inability to quickly dry the water content in the particles leads to the formation of a high-temperature area in the central core of particles [34,41]. The vapor pressure causes the vapors to escape from the particles, resulting in cracks and pores. In addition, the rapid heating of iron minerals and the slow heating of quartz generate thermal stress between different mineral phases, which also accelerates the production of cracks [42–44]. These pores and cracks provide a pathway for CO to deeply penetrate the particles, increasing the contact area between CO and ore [45]. This phenomenon accelerates the mineral phase reconstruction of iron-bearing minerals within the particles [46]. Furthermore, the pores and cracks effectively shorten the magnetization roasting time. The microwave treatment causes the formation of cracks between different minerals, which subsequently exposes the iron-bearing minerals.

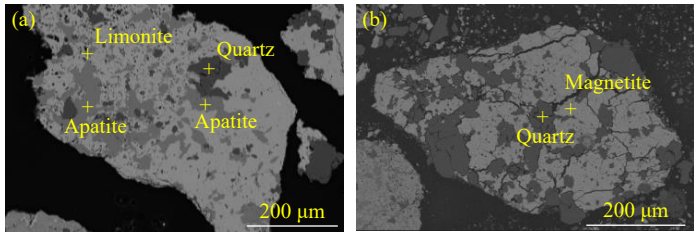

Fig. 4. SEM images of raw ore (a) and roasted products (b).

The pore structures of the limonite with different roasting times were characterized by N_2 isothermal adsorption and desorption curves. The specific surface area, average pore diameter distribution, and pore volume were analyzed by Brunauer–Emmett–Teller (BET) and Barret–Joyner–Halenda (BJH) method, and the results are shown in Fig. 5. The physical adsorption isotherms of the roasted limonite products are classified as type II, which indicates an unrestricted monolayer to multilayer adsorption. The hysteresis loop belongs to type H3, indicating that the pores of the roasted product have cracks and a plate-like slit, wedge-shaped structure [47–48]. Saturation adsorption is not evident in the areas with relatively high pressure, indicating that the pore structure is extremely irregular.

Fig. 5(a)–(e) is the N_2 adsorption and desorption curves of the limonite roasting products. When the roasting time is prolonged, the saturation adsorption amount and hysteresis ring area of N_2 increase. Therefore, roasting causes the minerals to

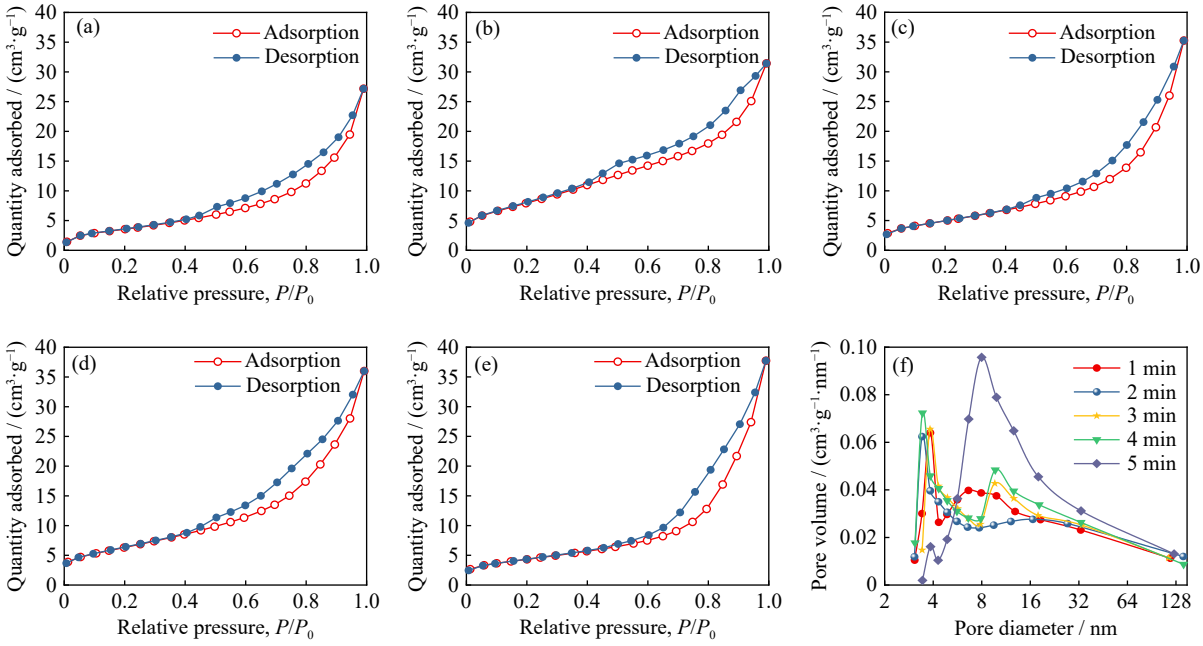

Fig. 5. N_2 adsorption–desorption curves of limonite microwave-roasted for 1 min (a), 2 min (b), 3 min (c), 4 min (d), and 5 min (e); (f) pore diameter distributions of limonite roasted for different times.

produce pores and cracks, which are conducive to the spread from the surface of the mineral to the inside and have a positive effect on magnetization roasting. As shown in Fig. 5(f), the pore diameter of the limonite roasting products is mainly in the range of 2–10 nm, and the pore type is mainly mesoporous. At the early stage of roasting, a peak appears at 3–4 nm, which may be the pore produced due to the dehydration of limonite. With the increase in roasting time, a new peak appears at 8–18 nm, and the roasting product begins to produce cracks. After roasting for 5 min, the peak at 3–4 nm basically disappears, and the peaks at 8–18 nm are enlarged, which may be due to the continuous production of new cracks merging with the original pore. These experiment results are consistent with the SEM. Table 2 illustrates that as the roasting time was prolonged from 1 to 5 min, the BET-specific surface area of the roasted product increases from 18.643 to 29.542 $m^2 \cdot g^{-1}$, the average pore diameter of the BJH slightly increases to 3.835 nm, and the total pore volume remains at approximately 0.053 $cm^3 \cdot g^{-1}$.

Table 2. Pore structure parameters of limonite subjected to microwave magnetization roasting for different times

Roasting time / min	BET specific surface area / ($m^2 \cdot g^{-1}$)	Total pore volume / ($cm^3 \cdot g^{-1}$)	BJH average pore diameter / nm
1	18.643	0.052	3.434
2	20.271	0.054	3.836
3	21.239	0.056	3.840
4	25.639	0.054	3.823
5	29.542	0.053	3.835

3.3. Phase transition analysis

The phases of products at different roasting times were explored under the roasting temperature of 773 K to explore the phase transformation of limonite, and the results are shown in Fig. 6. The sample has a high quartz content, and the diffraction peaks in the entire roasting process are still strong, indicating that the quartz has not changed. After roasting for 1 min, the diffraction peaks of goethite essentially disappear, and those of hematite slightly strengthen, indicating the dehydration transformation of goethite into hematite [44]. With the extension of the roasting time, the intensity of the diffraction peaks of hematite continuously decreases, new diffraction peaks of magnetite are generated, and the diffraction intensity gradually increases [49]. The diffraction peak of hematite disappears at a roasting time of 5 min, indicating that hematite has completely transformed into magnetite during the roasting. When the roasting time is extended to 6 min, the diffraction peaks in the XRD pattern are not significantly different from those of the sample roasted for 5 min. Furthermore, the absence of Fe diffraction peaks indicates that excessive reduction of the sample did not occur under these conditions.

3.4. Kinetic analysis

Kinetics is a crucial methodology for elucidating the variables that affect the reaction rate [50]. This study determined

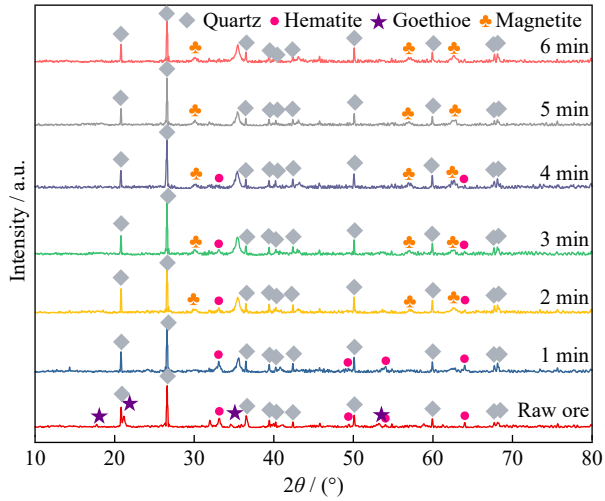

Fig. 6. XRD patterns of limonite products with different roasting times.

the characteristics of isothermal reduction kinetics by analyzing the FeO content in the roasted products.

Fig. 7(a) shows that within the range of the experiment, the α of limonite is positively correlated with the roasting temperature and roasting time; that is, increasing the roasting temperature and time will enhance the α of limonite. Fig. 7(b) illustrates that the v of limonite changes slowly in the preheating stage, probably because the sample temperature has not reached the preset temperature. After preheating, v increases sharply and then gradually decreases. At the initial stage of roasting, the limonite content in the system and the opportunity for contact between CO and limonite are high, resulting in rapid magnetization roasting. Over time, the limonite transforms to magnetite, and the principal reactant changes from the surface-exposed limonite to the newly uncovered limonite in the pores and cracks, leading to a gradual decrease in v. The kinetic analysis demonstrates that increasing the roasting temperature is conducive to enhancing v, thereby accelerating the magnetization roasting and shortening the roasting time. The v of magnetite reaches 100% during roasting at a temperature of 773 K for 5 min.

Fig. 7(c) shows the results of fitting α with the integral form of the mechanism function of each reaction kinetic model. In combination with the characteristics of each model and the properties of ores, this figure indicates that the reaction kinetic model is the diffusion model ($G(\alpha) = \alpha^2$) and the average value of R_2 reaches 0.945, corresponding to the mechanism function of $G(\alpha) = \alpha^2$. Calculations were performed by substituting α into $G(\alpha) = \alpha^2$, and the calculated values were linearly fitted to the reaction duration t to obtain the reaction rate constant k under different temperatures, as detailed in Table 3. $1/T$ and $\ln k$ were then substituted into Eq. (4) linear fitting to obtain the regression equation $y = -2446.97x - 2.5$, and the R^2 of this regression equation was 0.92612. The E_a, A, and k of the reaction are deduced to be 20.3441 $kJ \cdot mol^{-1}$, 0.08208 s^{-1}, and $0.08208\exp[-20.3441/(R_gT)]$, respectively. The E_a of limonite subjected to microwave fluidization roasting is lower than the E_a (29.62 $kJ \cdot mol^{-1}$) of roasting limonite reported in the literature, indic-

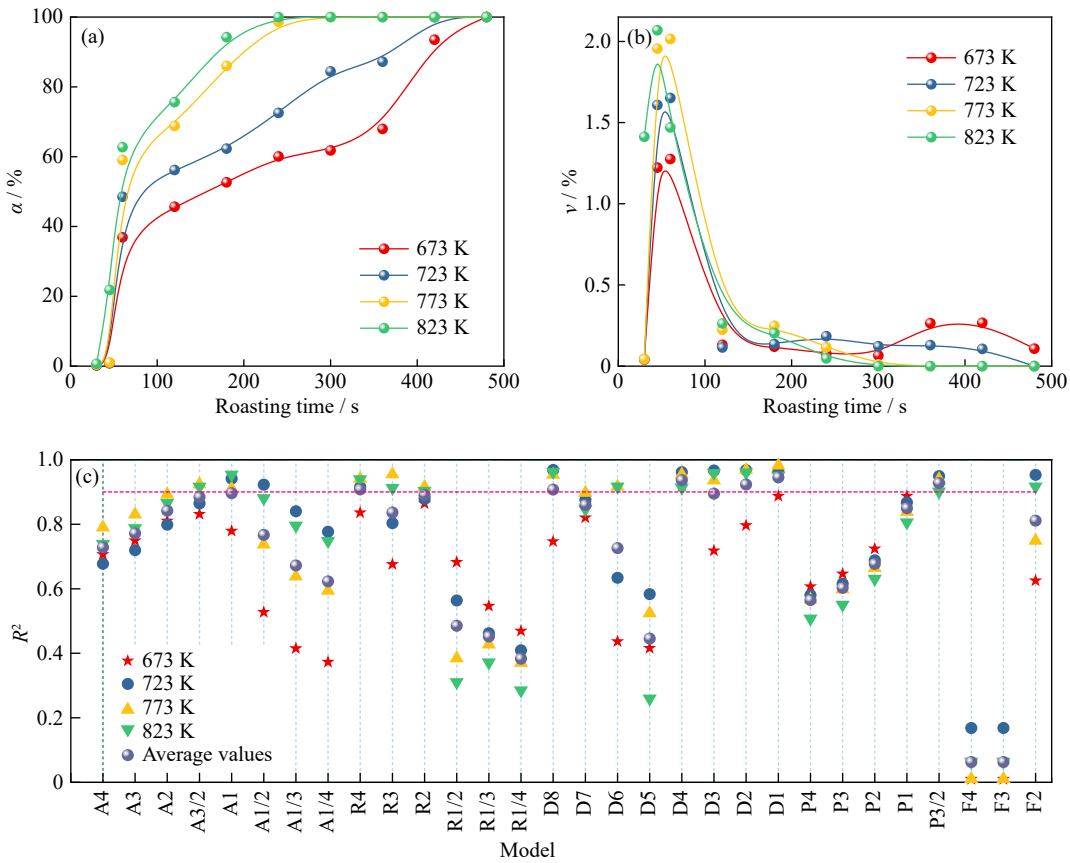

Fig. 7. Thermodynamic analysis of the microwave fluidization roasting of limonite: (a) *α*, (b) *v*, and (c) R^2 for different mechanistic function fits.

ating that microwave heating increases the rate of reduction reaction [11]. In addition, the reaction with E_a above 40 kJ·mol^{-1} is controlled by chemical reactions, that with E_a below 20 kJ·mol^{-1} is controlled by diffusion, and that with E_a between 20 and 40 kJ·mol^{-1} is synergistically controlled by chemical reactions and diffusion [51–53]. On the basis of this theory, the fluidization magnetization roasting of limonite by microwave heating is synergistically controlled by chemical reaction and diffusion.

Table 3. *k* and R^2 of microwave fluidization roasting at various temperatures

No.	Roasting temperature / K	k / s^{-1}	R^2
1	673	0.00213	0.88696
2	723	0.00271	0.96209
3	773	0.00389	0.98203
4	823	0.00391	0.95070

3.5. Magnetic property analysis

The main purpose of limonite magnetization roasting is to transform the ferrimagnetic minerals hematite and goethite into ferromagnetic mineral magnetite to create favorable conditions for the subsequent magnetic separation. The products roasted at varying temperatures were analyzed using a VSM to investigate the evolution of the magnetic properties of limonite subjected to microwave roasting. Fig. 8 shows the magnetization and specific magnetization coefficient of the limonite microwave roasting products at different temperatures. The magnetic properties of the roasted products increase when the roasting temperature increases from 623 to 773 K. After roasting at 773 K, the saturation magnetization of the roasted product increases from 0.95 A·m^2·kg^{-1} for the raw ore to 23.08 A·m^2·kg^{-1}, and the maximum specific magnetization coefficient increases from 4.27 × 10^{-5} to 2.50 × 10^{-4} m^3·kg^{-1}. When the temperature is 823 K, the magnetic properties of the roasted product decrease slightly. Combined with thermodynamic analysis, this finding suggests the partial reduction of magnetite to wüstite by CO.

3.6. Microwave fluidization magnetization roasting and magnetic separation

Magnetic field intensity is the primary external factor affecting the final magnetic separation indicators of ores. Therefore, the roasted products obtained under a temperature of 773 K and a roasting time of 5 min were used to study the effect of the magnetic field intensity on the magnetic separation of iron ores. Magnetic field intensity condition experiments were conducted under the condition that −45 μm particle size accounted for 75wt% of the ores, and the experimental results are shown in Fig. 9. With the increase in magnetic field intensity, the iron recovery gradually increases. After the magnetic field intensity reaches 120 kA·m^{-1}, the iron recovery is stable at approximately 90wt%, and the iron grade remains at 59wt%. Under the magnetic field intensity of 120 kA·m^{-1}, a magnetic concentrate with an iron grade of

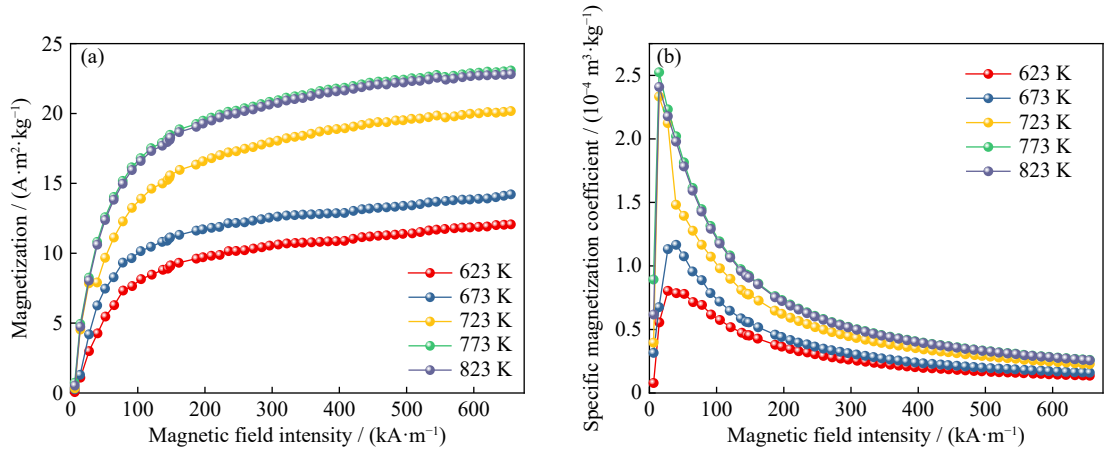

Fig. 8. Magnetization (a) and specific magnetization coefficient (b) of limonite products roasted at different temperatures.

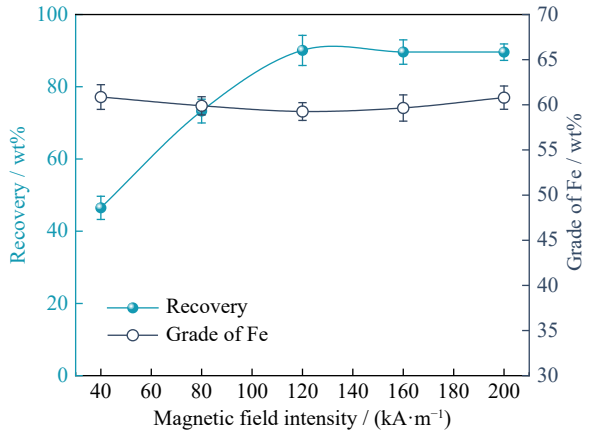

Fig. 9. Effect of magnetic field intensity on the magnetic separation of microwave fluidization magnetization roasting products of limonite ores.

59.26wt% and iron recovery of 90.07wt% is obtained.

3.7. Discussion

Laboratory magnetic separation experiments confirmed the feasibility of using microwave fluidization roasting for limonite ores. This method offers several advantages over traditional roasting technologies. The ability to absorb microwaves in the material mainly depends on the material's dielectric properties. Among the main minerals in this iron ore, the complex dielectric constant decreases in the order of magnetite > hematite > quartz. As a strong polar molecule, water significantly influences the dielectric properties of iron ore [54]. The microwave fluidization roasting of limonite has three key benefits: (1) different microwave heating rates and certain selective heating effects, (2) high water content of limonite ore, and (3) fluidization accelerating the mass transfer effect and facilitating contact between the ore and CO. The morphological changes and mineral phase transformation during the microwave fluidization magnetization roasting of limonite are shown in Fig. 10. During roasting, the water with a high dielectric loss factor is the first to heat up and escape in the form of vapors, leading to the formation of pores on the limonite surface. At the same time, goethite is transformed into hematite. The rapid heating of hematite and the newly transformed magnetite results in thermal stresses on the iron-bearing minerals and quartz, which further produce cracks and accelerate the reduction roasting. Moreover, microwave energy is clean and efficient, offering the benefit of nonpollution. Microwave heating selectively targets

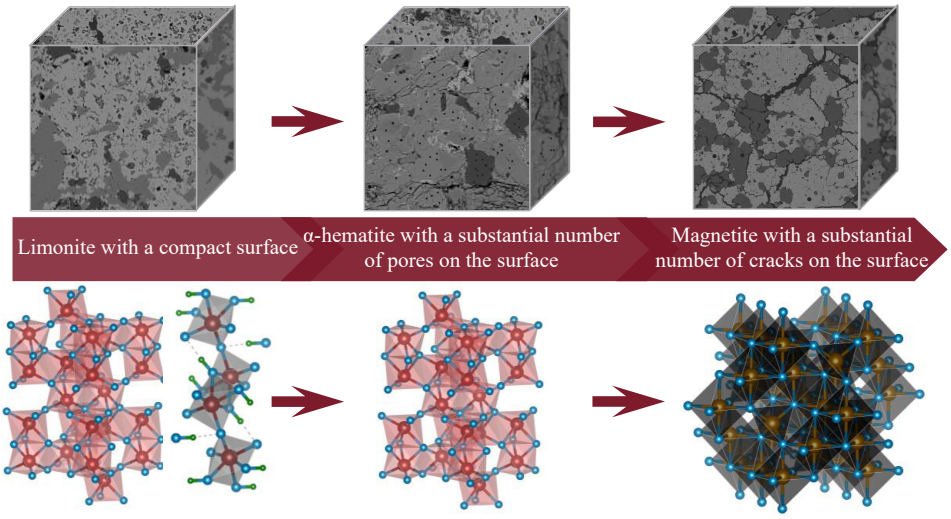

Fig. 10. Schematic of morphological changes and mineral phase transformation during the microwave fluidization magnetization roasting of limonite.

phases with high dielectric losses, thus enhancing energy utilization efficiency. At present, the high cost of microwave heating equipment is the primary barrier to the widespread adoption of microwave roasting technology [55].

4. Conclusions

In this work, microwave fluidization roasting was employed to process refractory limonite. The microstructure and mineral phase transformations of the roasted products were analyzed, and isothermal kinetic studies were conducted. The key findings are summarized below.

(1) The mineral phase transformation path of limonite is mainly FeO(OH) to α-Fe_2O_3 and finally to Fe_3O_4. The roasted product achieved a saturation magnetization of 23.08 $A \cdot m^2 \cdot kg^{-1}$ and a maximum specific magnetization coefficient of 2.50×10^{-4} $m^3 \cdot kg^{-1}$.

(2) With the use of magnetic separation at a magnetic field intensity of 120 $kA \cdot m^{-1}$, an iron concentrate with an Fe grade of 59.26wt% and recovery of 90.07wt% was obtained after roasting for 5 min at 773 K.

(3) The kinetic mechanism underlying the microwave-assisted fluidization magnetization roasting of limonite followed a diffusion model ($G(\alpha) = \alpha^2$). The apparent activation energy of the reaction was 20.3441 $kJ \cdot mol^{-1}$, and the preexponential factor was 0.08208 s^{-1}, indicating that the reaction is synergistically controlled by chemical reaction and diffusion.

Acknowledgements

This work was financially supported by the National Key Research and Development Program of China (No. 2021YFC2901000), the National Natural Science Foundation of China (No. 52104249), the Liaoning Joint Fund General Support Program Project (No. 2023-MSBA-126), and the Fundamental Research Funds for the Central Universities (No. N2401019).

Conflict of Interest

The authors confirm that they have no competing interests or financial ties that could influence the outcomes or interpretation of this research.

Supplementary Information

The online version contains supplementary material available at https://doi.org/10.1007/s12613-024-3018-1.

References

[1] S.J. Liu and M.H. Lin, Trade dynamics of ferrous metals in emerging and developing countries, *Resour. Policy*, 90(2024), art. No. 104742.

[2] R. Chaurasiya, G. Mukhopadhyay, and P. Maji, Comparative analysis of high cycle fatigue performance of HS1000 and C80 steel, *Mater. Today Proc.*, (2024). DOI: 10.1016/j.matpr.2024.05.112

[3] E. Mokhtari, A. Heidarpour, and F. Javidan, Mechanical performance of high strength steel under corrosion: A review study, *J. Constr. Steel Res.*, 220(2024), art. No. 108840.

[4] Q. Zhang, Y.S. Sun, Y.X. Han, Y.J. Li, and P. Gao, Review on coal-based reduction and magnetic separation for refractory iron-bearing resources, *Int. J. Miner. Metall. Mater.*, 29(2022), No. 12, p. 2087.

[5] A.A. Neisiani, R. Saneie, A. Mohammadzadeh, D.G. Wonyen, and S.C. Chelgani, Biodegradable hematite depressants for green flotation separation–An overview, *Miner. Eng.*, 199(2023), art. No. 108114.

[6] S.K. Roy, D. Nayak, and S.S. Rath, A review on the enrichment of iron values of low-grade Iron ore resources using reduction roasting–magnetic separation, *Powder Technol.*, 367(2020), p. 796.

[7] H.Y. Sun, M.J. Zhang, Z. Zou, and D. Yan, Fluidized magnetization roasting utilization of refractory siderite-containing iron ore with low gas reduction potential, *Adv. Powder Technol.*, 34(2023), No. 5, art. No. 103994.

[8] Z.D. Tang, Y.X. Han, Y. Cao, Y.S. Sun, and P. Gao, Clean recycling of low-grade refractory limonitic waste using suspension magnetization roasting coupled with magnetic separation: A semi-industrial approach towards a waste utilization plan, *Process. Saf. Environ. Prot.*, 173(2023), p. 61.

[9] P. Chen, T.H. Chen, Q.Q. Xie, L. Xu, H.B. Liu, and Y.F. Zhou, Mineralogy and geochemistry of limonite as a weathering product of ilvaite in the Yeshan iron deposit, Tongling, China, *Clays Clay Miner.*, 66(2018), No. 2, p. 190.

[10] W.F. Souza, I.R. Guimarães, D.Q. Lima, C.L.T. Silva, and L.C.A. Oliveira, Brazilian limonite for the oxidation of quinoline: High activity after a simple magnetic separation, *Energy Fuels*, 23(2009), No. 9, p. 4426.

[11] P.F. Liu, X.R. Zhu, Y.X. Han, Y.J. Li, and P. Gao, Fluidization magnetization roasting of limonite ore using H_2 as a reductant: Phase transformation, structure evolution, and kinetics, *Powder Technol.*, 414(2023), art. No. 118107.

[12] V. Nunna, S.P. Suthers, M.I. Pownceby, and G.J. Sparrow, Beneficiation strategies for removal of silica and alumina from low-grade hematite–goethite iron ores, *Miner. Process. Extr. Metall. Rev.*, 43(2022), No. 8, p. 1049.

[13] Y.S. Sun, X.L. Zhang, Y.X. Han, and Y.J. Li, A new approach for recovering iron from iron ore tailings using suspension magnetization roasting: A pilot-scale study, *Powder Technol.*, 361(2020), p. 571.

[14] X. Zhang, S.Y. He, H.Y. Sun, Q.S. Zhu, J. Li, and H.Z. Li, Mechanism of surface morphology evolution in the reduction of fine iron ore in a conical fluidized bed reactor, *Chem. Eng. Sci.*, 220(2020), art. No. 115468.

[15] Y.F. Yu and C.Y. Qi, Magnetizing roasting mechanism and effective ore dressing process for oolitic hematite ore, *J. Wuhan Univ. Technol. Mater. Sci. Ed.*, 26(2011), No. 2, p. 176.

[16] S.R. Mohanty, S. Yadav, and A.K. Shukla, A techno-economic approach for magnetising roasting of iron ore composite pellet using conventional and hybrid microwave furnace, *Chem. Eng. Process. Process Intensif.*, 191(2023), art. No. 109444.

[17] E. Ireland, K. Pitt, and R. Smith, A review of pulsed flow fluidisation; the effects of intermittent gas flow on fluidised gas–solid bed behaviour, *Powder Technol.*, 292(2016), p. 108.

[18] Z.D. Tang, P.Y. Li, P. Gao, Y.J. Li, and Y.X. Han, Minerals phase transformation by hydrogen reduction technology: A new approach to recycle iron from refractory limonite for reducing carbon emissions, *Adv. Powder Technol.*, 33(2022), No. 12, art. No. 103870.

[19] Y.S. Sun, X.R. Zhu, Y.X. Han, Y.J. Li, and P. Gao, Iron recovery from refractory limonite ore using suspension magnetization roasting: A pilot-scale study, *J. Cleaner Prod.*, 261(2020), art. No. 121221.

[20] M.F. Pinheiro, J.I.S. da Silva, C.N. de Oliveira, *et al.*, Multivariate modeling and optimization of the reverse cationic flotation process of iron ore using depressant-modified starch, *Miner. Eng.*, 205(2024), art. No. 108485.

[21] R. Sehati, M.R.S. Yazdi, and A.H. Omran, Assessment of the effect of iron magnetic concentrate desulfurization by flotation method on the quality of green and cooked pellets: A laboratory and pilot-scale study, *Miner. Eng.*, 202(2023), art. No. 108269.
[22] X.L. Zhang, Z.Y. Zhou, P. Gao, and Y.X. Han, Enhanced iron extraction from high-phosphorus waste limonite ore via suspension magnetization roasting: A pilot-scale study, *J. Cleaner Prod.*, 424(2023), art. No. 138860.
[23] J.L. Ning, P. Gao, Y. Wang, *et al*., Mineralogical characterization and flotation properties of rare earths in refractory iron tailings subjected to hydrogen-based mineral phase transformation, *Int. J. Miner. Metall. Mater.*, 32(2025), No. 6, p. 1309.
[24] R.F. Wang, S. Yuan, Y.J. Li, P. Gao, and R. Li, Hydrogen-based mineral phase transformation mechanism investigation of pyrolusite ore, *Int. J. Miner. Metall. Mater.*, 31(2024), No. 11, p. 2445.
[25] Y.L. Wang, C.H. Liu, Y.W. Li, Y.Q. Ye, F.C. Xu, and Y.Y. Li, Metallic antimony preparation by carbothermic reduction of stibnite concentrates: Strategies, mechanisms, and comparison of microwave and conventional roasting, *Miner. Eng.*, 208(2024), art. No. 108584.
[26] C. Valverde, M.M. Rodríguez-García, E. Rojas, and R. Bayón, State of the art of the fundamental aspects in the concept of microwave-assisted heating systems, *Int. Commun. Heat Mass Transf.*, 156(2024), art. No. 107594.
[27] A. Mohanty and S.K. Panigrahi, RETRACTED: Optimizing microwave energy utilization & heating efficiency: Comparative analysis of susceptor materials for enhanced microwave absorption performance, *Int. J. Therm. Sci.*, 203(2024), art. No. 109082.
[28] A. Hapid, S. Zullaikah, M. Mahfud, *et al*., Optimization of microwave-assisted roasting: Box-behnken design for oxidation of sulfide minerals and control of atmospheric sulfur in refractory gold ore pretreatment, *Case Stud. Chem. Environ. Eng.*, 10(2024), art. No. 100826.
[29] N. Mizuno, S. Kosai, and E. Yamasue, Microwave-based extractive metallurgy to obtain pure metals: A review, *Clean. Eng. Technol.*, 5(2021), art. No. 100306.
[30] E. Colombini, R. Rosa, L. Trombi, M. Zadra, A. Casagrande, and P. Veronesi, High entropy alloys obtained by field assisted powder metallurgy route: SPS and microwave heating, *Mater. Chem. Phys.*, 210(2018), p. 78.
[31] S.K. Roy, D. Nayak, N. Dash, N. Dhawan, and S.S. Rath, Microwave-assisted reduction roasting–magnetic separation studies of two mineralogically different low-grade iron ores, *Int. J. Miner. Metall. Mater.*, 27(2020), No. 11, p. 1449.
[32] W.T. Zhou, Y.S. Sun, Y.X. Han, P. Gao, and Y.J. Li, Mechanism of microwave assisted suspension magnetization roasting of oolitic hematite ore, *J. Cent. South Univ.*, 29(2022), No. 2, p. 420.
[33] F.F. Wu, Z.F. Cao, S. Wang, and H. Zhong, Phase transformation of iron in limonite ore by microwave roasting with addition of alkali lignin and its effects on magnetic separation, *J. Alloy. Compd.*, 722(2017), p. 651.
[34] T. Le, S.H. Ju, J.H. Peng, *et al*., Comparison of microwave roasting on wet/dry mixture of diasporic bauxite with alkaline: Revealing the intensifying effect of H_2O on chemical reaction, *J. Microw. Power Electromagn. Energy*, 50(2016), No. 4, p. 217.
[35] J.L. Tian, B.S. Chen, H.Y. Xia, W.Z. Yang, and L.B. Zhang, Response surface methodology was used to optimize the defluorination process of steam-enhanced microwave roasting waste cathode carbon, *Chem. Eng. Process. Process Intensif.*, 204(2024), art. No. 109955.
[36] X. Li, Y.B. Liu, W.J. Yang, B.Z. Ma, Y.Q. Chen, and C.Y. Wang, Phase transformation and roasting kinetics of cobalt-rich copper sulfide ore in oxygen atmosphere assisted by sodium sulfate, *J. Ind. Eng. Chem.*, 116(2022), p. 217.
[37] M.Q. Wei, Q.B. Yu, W.J. Duan, *et al*., CO_2 desorption kinetics for waste ion-exchange resin-based activated carbon by model-fitting and model-free, *Thermochim. Acta*, 655(2017), p. 52.
[38] W.B. Li, J.J. Chen, S.K. Cheng, J.Y. Sun, and X.L. Zhang, Thermal decomposition mechanism and kinetics of bastnaesite in suspension roasting process: A comparative study in N_2 and air atmospheres, *J. Rare Earths*, 42(2024), No. 9, p. 1809.
[39] Z.Y. Zhou, X.L. Zhang, W.B. Li, *et al*., An innovation for strengthen iron extraction from phosphorus-bearing refractory iron ore via suspension magnetization roasting and flotation, *Adv. Powder Technol.*, 35(2024), No. 4, art. No. 104382.
[40] T.A. Atia and J. Spooren, Microwave assisted alkaline roasting-water leaching for the valorisation of goethite sludge from zinc refining process, *Hydrometallurgy*, 191(2020), art. No. 105235.
[41] T. Le, S.H. Ju, S. Koppala, *et al*., Kinetics study of microwave enhanced reactions between diasporic bauxite and alkali solution, *J. Alloy. Compd.*, 749(2018), p. 652.
[42] P. Hartlieb, F. Kuchar, P. Moser, H. Kargl, and U. Restner, Reaction of different rock types to low-power (3.2 kW) microwave irradiation in a multimode cavity, *Miner. Eng.*, 118(2018), p. 37.
[43] H.Y. Li, J. Wang, X.J. Zhu, *et al*., Basic research on the microwave absorbing properties and microwave roasting kinetic of cyanide tailings, *Powder Technol.*, 401(2022), art. No. 117346.
[44] V. Nunna, S. Hapugoda, M.I. Pownceby, and G.J. Sparrow, Beneficiation of low-grade, goethite-rich iron ore using microwave-assisted magnetizing roasting, *Miner. Eng.*, 166(2021), art. No. 106826.
[45] S. Sudhir, S. Soren, G.M. Chowdhury, *et al*., Utilization of rice husk substituting fossil fuel for pelletization process of goethite iron ore, *Environ. Technol. Innov.*, 34(2024), art. No. 103597.
[46] H.H. Zhang, P. Gao, S. Yuan, and Y.H. Qin, Enhancement of magnetization roasting of hematite ore by high voltage pulse discharge, *Miner. Eng.*, 203(2023), art. No. 108360.
[47] M.X. Wang, Q. Zhang, Y.S. Sun, Y.X. Han, and P. Gao, Green iron recovery through hydrogen-based mineral phase transformation using ultrafast air-cooling for heat recycling: A pilot-scale investigation, *J. Clean. Prod.*, 450(2024), art. No. 141867.
[48] J.H. He, P. Gao, S. Yuan, *et al*., High efficiency separation of bastnaesite ($REFCO_3$) and monazite ($REPO_4$) in mixed rare earth concentrate by heating under N_2 and leaching with $HCl/AlCl_3$, *Hydrometallurgy*, 228(2024), art. No. 106338.
[49] S. Yuan, H.X. Xiao, R.F. Wang, Y.J. Li, and P. Gao, Improved iron recovery from low-grade iron ore by efficient suspension magnetization roasting and magnetic separation, *Miner. Eng.*, 186(2022), art. No. 107761.
[50] J. Cheng, H.Y. Li, D. Hai, X.M. Chen, J. Diao, and B. Xie, Magnesiation roasting kinetics exploration of vanadium slag toward minimization of tailing toxicity, *J. Hazard. Mater.*, 452(2023), art. No. 131378.
[51] H.Y. Li, S.W. Li, J.H. Peng, C. Srinivasakannan, L.B. Zhang, and S.H. Yin, Ultrasound augmented leaching of nickel sulfate in sulfuric acid and hydrogen peroxide media, *Ultrason. Sonochem.*, 40(2018), p. 1021.
[52] H.Y. Li, L.B. Zhang, H.M. Xie, *et al*., Ultrasound-assisted silver leaching process for cleaner production, *JOM*, 72(2020), No. 2, p. 766.
[53] H.L. Long, H.Y. Li, P.C. Ma, *et al*., Effectiveness of thermal treatment on Pb recovery and Cl removal from sintering dust, *J. Hazard. Mater.*, 403(2021), art. No. 123595.
[54] J.W. Walkiewicz, G. Kazonich, and S.L. McGill, Microwave heating characteristics of selected minerals and compounds, *Miner. Metall. Process.*, 5(1988), No. 1, p. 39.
[55] J.W. Yu, Y.X. Han, Y.J. Li, and P. Gao, Recent advances in magnetization roasting of refractory iron ores: A technological review in the past decade, *Miner. Process. Extr. Metall. Rev.*, 41(2020), No. 5, p. 349.